AIAA JOURNAL
Vol. 41, No. 5, May 2003

Prediction of Lobed Mixer Vortical Structures with a $k-\epsilon$ Turbulence Model

Hayder Salman,* Gary J. Page,† and James J. McGuirk‡
Loughborough University, Loughborough, England LE11 3TU, United Kingdom

Numerical simulations of an incompressible planar shear layer and a lobed mixer flowfield are presented and validated against the detailed experimental measurements of McCormick and Bennett (McCormick, D. C., and Bennett, J. C., Jr., "Vortical and Turbulent Structure of a Lobed Mixer Free Shear Layer," *AIAA Journal*, Vol. 32, No. 9, 1994, pp. 1852–1859). The study focused on quantifying the predictability of these flows using the standard $k-\epsilon$ turbulence model. Simulations for the planar shear layer showed that, whereas the self-similar behavior can be captured by the model, the measured near-field development of the shear layer could not be reproduced in the simulations. Inconsistencies between simulations and experiments arise as a result of the Kelvin–Helmholtz instability that is not captured in the simulations. Predictions for the lobed mixer shear layer revealed a lag of 1.75 lobe heights in the shear-layer development with respect to the measured data. Global parameters such as momentum thickness and streamwise circulation generally showed an underprediction of 20% and an overprediction of 65% with respect to measured values, respectively. Good prediction of the primary Reynolds shear stresses that control the variation of the momentum thickness was obtained. An analysis for the equation of the streamwise component of vorticity revealed that the important contribution to the streamwise circulation decay rate is the secondary shear stress and the normal stress anisotropy. Neither is well predicted by the $k-\epsilon$ model, leading to poorer predictions of the streamwise circulation decay rate.

Introduction

WHEN two coflowing streams separated by a splitter plate with different velocities interact, a mixing layer is formed. Mixing layers are one example of a class of flows where mixing and transport is an intrinsic part of the problem. An extensive amount of work can therefore be found in the literature on this type of flow (e.g., Ho and Huerre[1]). Mixing layers are a common feature of lobed mixer flows that are often found in gas turbine engines. Lobed mixers essentially consist of a splitter plate with a corrugated trailing edge. The purpose of these devices is to mix the bypass and core flows together in the shortest possible distance with minimum pressure losses,[2] thereby reducing jet noise. Studies by Bevilaqua[3] and Paterson[4] have revealed that lobed mixers achieve rapid mixing of the two streams by producing a spanwise array of large-scale vortical structures downstream of the mixer. This arises in response to the radial deflections the flow experiences as it passes over the mixer surface. The resulting flow is a highly complex three-dimensional convoluted shear layer.

There is a great deal of interest in simulating lobed mixer flows. One impetus for doing so is that designing an optimum mixer on experimental evidence alone is expensive and nontrivial because of the wide range of mixer parameters that can be varied. By exploiting computational approaches, some of these costs can be reduced. Computational studies of lobed mixers to date have employed a hierarchy of numerical methods. These range from reduced-order point vortex models, as in Strickland et al.,[5] to the solution of the Reynolds-averaged form of the Navier–Stokes equations as in Koutmos and McGuirk.[6] The Reynolds-averaged equations introduce additional unknowns, and to close the system approximations in the form of turbulence models are used. The most commonly used turbulence model for lobed mixer simulations has been the standard linear $k-\epsilon$ model of Launder and Spalding.[7] However, there appears to be little justification in the literature for the use of the $k-\epsilon$ model as sufficient for capturing the mixing in lobed mixer flows. The first simulation of the flow around a lobed mixer geometry employing this model was performed by Koutmos and McGuirk.[6] Following this, a number of papers have appeared that employ the same turbulence model, including the work of Malecki and Lord,[8] Abolfadl and Sehra,[9] Tsui and Wu,[10] and O'Sullivan et al.[11] Of these, only the studies of Tsui and Wu and of Koutmos and McGuirk appear to contain thorough validations of the computations against experimental data. The work of Tsui and Wu did not, however, resolve the flow through the mixer. The results within the mixing duct were therefore strongly dependent on the accuracy of the measurements at the mixer's trailing edge, which were used to provide the inlet boundary conditions in the computations. The computations of Koutmos and McGuirk therefore appear to be the best available validation study of the $k-\epsilon$ turbulence model for this flow. The use of coarse cylindrical grids in their calculations, however, raises uncertainties with regard to the numerical accuracy both within the mixing duct and over the mixer surfaces. Adding to this the lack of comparisons made for global parameters such as the momentum thickness or streamwise circulation, which are important in quantifying the level of mixing; their study cannot be regarded as completely conclusive.

In response to these concerns, Salman et al.[12] attempted a validation study using the lobed mixer of Yu and Yip.[13] The mixer was purposefully chosen because of the high resolution of measurements taken of the mean and turbulent flowfield of the mixer. The work adopted two independent mathematical models. The first constituted the Reynolds-averaged form of the Navier–Stokes equations with the standard $k-\epsilon$ model. The second was an inviscid point vortex model to study the stability of the vortex array produced by the Yu and Yip mixer configuration. This study revealed that strong sidewall effects were present causing lateral movements and distortions of the vortices. Consequently, this raised difficulties in choosing a well-defined region for integrating the vorticity, and thus it was not possible to quantify the decay rate of the vortex strength. In addition, no clear conclusions could be made with regard to the accuracy of the predicted turbulent field. To circumvent these difficulties, an alternative mixer is studied here and corresponds to the symmetric mixer

Received 9 April 2002; revision received 4 November 2002; accepted for publication 11 November 2002.

*Research Assistant, Department of Aeronautical and Automotive Engineering; currently Research Associate, Room 3-449c, Department of Mechanical Engineering, Massachusetts Institute of Technology, 77 Massachusetts Avenue, Cambridge, MA 02139; hsalman@mit.edu.

†Lecturer, Department of Aeronautical and Automotive Engineering.

‡Professor of Aerodynamics, Department of Aeronautical and Automotive Engineering.

configuration studied experimentally by McCormick and Bennett[14] (see also McCormick[15] for more details). An important criterion set by Salman et al.[12] is that the lobed mixer array should meet the tunnel side walls at lobe peaks or troughs to reduce the end-wall effects on the evolving streamwise vortical structures. The mixer of McCormick passes this criteria and is therefore chosen for the present study.

The aim of the work conducted here is to assess and quantify the applicability of the k–ϵ turbulence model to lobed mixer flows and to identify the key processes that must be captured for accurate simulation of such flows. A complete evaluation of the turbulence model can only be obtained if variations in the velocity ratio and Reynolds number are included. Both Eckerle et al.[16] and Yu et al.[17] have experimentally observed that variations in the velocity ratio can significantly affect the mixing downstream of the lobed mixer. Detailed validations that include these effects can be used to show clearly the influence of the normal and streamwise vorticity on the flow. However, in this work we will focus on the mixer of McCormick and Bennett, which did not include variations in the aforementioned parameters. The aim in this work is therefore aimed at identifying the performance of the model under their particular flow conditions. To evaluate the model, two key objectives are addressed in this study. First, a detailed quantitative validation study is carried out to establish the level of agreement between predictions and experiments for lobed mixer flows. Although such detailed comparisons reveal the merits and pitfalls of the Reynolds-averaged k–ϵ model solution approach, it does not explain the cause of the discrepancies seen in the results. A second objective of this work is to identify the key processes driving this flow. This is achieved through an analysis of the governing flow equations to highlight specific features of the turbulence model that require improvement.

The paper begins with a description of the mathematical model. This is followed by a description of the mixer configuration of McCormick together with the discretization of the computational domain. Results are then presented for a benchmark planar shear layer also studied in McCormick's experiments. The lobed mixer results are then presented with a survey of mean flow quantities. The influence of the turbulent Reynolds stresses on the mean flow is discussed by referring back to the equations governing streamwise velocity and streamwise vorticity. Conclusions and recommendations for future work are given at the end of the paper.

Mathematical Model

The numerical approach is based on the solution of the full three-dimensional form of the Navier–Stokes equations in steady-state Reynolds-averaged form for constant density flows. These can be written using Cartesian tensor notation as

$$\frac{\partial \rho U_i}{\partial x_i} = 0 \tag{1}$$

$$\frac{\partial}{\partial x_j}(\rho U_i U_j + \rho \overline{u_i' u_j'}) = -\frac{\partial P}{\partial x_i} + \frac{\partial \tau_{ij}}{\partial x_j} \tag{2}$$

where

$$\tau_{ij} = \mu\left(\frac{\partial U_i}{\partial x_j} + \frac{\partial U_j}{\partial x_i}\right) \tag{3}$$

The Reynolds stresses ($\rho \overline{u_i' u_j'}$) in the preceding equations, which appear as a result of the Reynolds averaging, have been modeled using the standard high-Reynolds-number k–ϵ turbulence model of Launder and Spalding.[7]

The system of Eqs. (1) and (2), together with the turbulence model equations, comprise a closed set of equations. Solutions are obtained using a finite volume discretization. The formulation comprised a linearized implicit scheme using a base first-order upwind differencing, with second-order total-variation-diminishing-limited MUSCL-type differencing introduced as a deferred correction for the momentum and the turbulence model equations. The solution algorithm employed was based on the standard SIMPLE pressure–correction algorithm adapted to curvilinear multiblock structured grids using a collocated grid arrangement. For more details on the methodology, the reader is referred to Page et al.[18]

Mixer Configuration

Details of the mixer configuration studied are presented in Fig. 1. The important parameters that define a lobed mixer are the lobe wavelength λ, the lobe height H, and the lobe inclination angle α. A schematic is also presented to clarify the region where the lobes intersect the upstream flat plate. The wind-tunnel cross section used by McCormick and Bennett was 408 mm wide by 400 mm high.

Using this mixer definition, a grid was generated representing a computational domain for one half-lobe (defined from a lobe peak to a lobe trough) based on the assumption of symmetrical repetition of flow properties across the mixer. The computational domain extended 5.3 lobe wavelengths upstream and 44 wavelengths downstream of the mixer trailing edge. The grid generated consisted of 700,000 grid cells. This grid size was chosen following a grid-refinement study using another similar lobed mixer geometry as discussed in Salman.[19]

Figure 2 shows the mesh produced for the half-lobe geometry studied here. The mesh used in this study consisted of a seven-block multiblock structured grid allowing flexibility in controlling the grid quality. This is clearly demonstrated with the grids generated that maximize grid orthogonality within the mixing duct, whereas farther upstream, where the flow is less complex, grid orthogonality is sacrificed. This allows grids with minimized skewness to be generated in regions where the complex vortex structures formed, a feature often found difficult to achieve by other investigators (e.g., Rollin et al.[20]). The approach can reduce numerical diffusion quite significantly in the important shear-layer regions of the flow.

In this study comparisons with only the turbulent data of McCormick and Bennett are presented. The boundary conditions for the computations were therefore based on the test conditions of the turbulent flow used by McCormick and Bennett with the high- and low-speed streams set at velocities of 8.53 and 4.88 ms^{-1}, respectively. These conditions correspond to a velocity ratio (low-speed

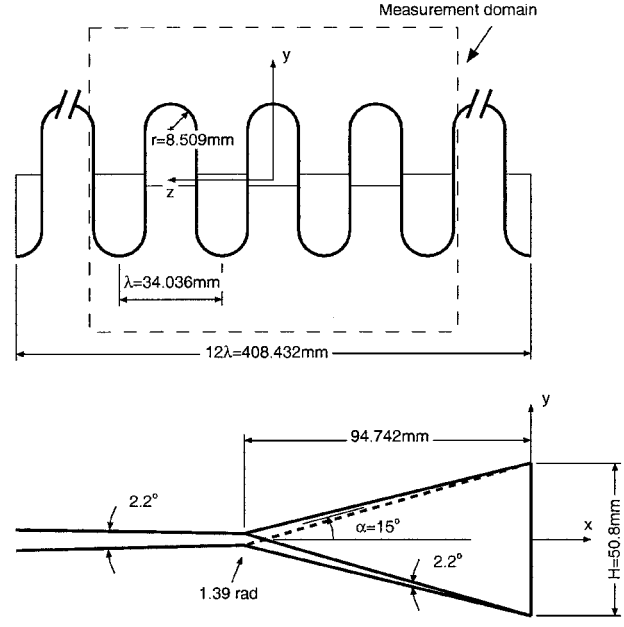

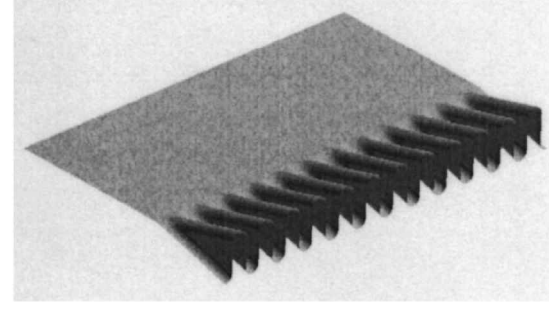

Fig. 1 Definition of mixer configuration investigated.

Table 1 Turbulent boundary-layer properties at $x = 0.0254$ m upstream of the plate's trailing edge: low-speed flow

Properties	U_∞, m/s	δ^*, m[a]	θ, m[b]	$H = \delta^*/\theta$[c]	Re_θ[d]
Experiments	4.88	0.00188	0.00124	1.524	392
Predictions	4.88	0.00172	0.00107	1.607	378

[a] δ^* = displacement thickness.
[b] θ = momentum thickness.
[c] H = shape factor.
[d] Re_θ = boundary-layer Reynolds number.

Table 2 Turbulent boundary-layer properties at $x = 0.0254$ m upstream of the plate's trailing edge: high-speed flow

Properties	U_∞, m/s	δ^*, m[a]	θ, m[b]	$H = \delta^*/\theta$[c]	Re_θ[d]
Experiments	8.53	0.00159	0.00111	1.438	617
Predictions	8.53	0.00169	0.00114	1.484	653

[a] δ^* = displacement thickness.
[b] θ = momentum thickness.
[c] H = shape factor.
[d] Re_θ = boundary-layer Reynolds number.

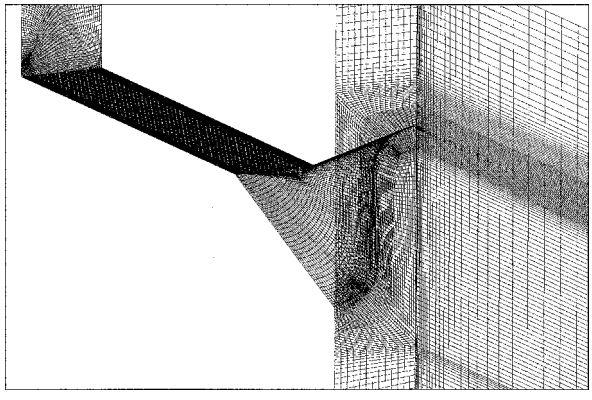

Fig. 2 Multiblock structured grid used in computations.

stream/high-speed stream) of 0.57 and an average freestream velocity U_r of 6.71 ms^{-1}. Freestream turbulence intensity levels of 2% were assumed. These values were therefore used to represent the inlet boundary conditions in the computational-fluid-dynamics (CFD) calculations. The value of the turbulent dissipation rate ϵ at inlet was calculated using a length scale based on half the wind-tunnel height. Constant profiles were assumed for mean and turbulent quantities in both streams. Tunnel walls were modeled as slip walls as this does not require the boundary layer to be resolved, thus reducing the mesh size.

Results and Discussion

Planar Shear Layer

The planar shear layer is ideal for benchmarking the k–ϵ turbulence model as it forms one of the basic flows used in its calibration. Any deficiencies found in the model for this simple flow can be separated at this early stage from any other physical processes that the model might not be able to capture in the complex convoluted shear layers of lobed mixers. Therefore, this simplified problem serves as a good starting point in the investigation of turbulence models for convoluted shear layers. In calibrating the k–ϵ turbulence model interest is often given to achieving the correct self-similar behavior in the far field. For lobed mixer flows, however, the shear-layer development in the near field is of more interest. To allow results of the planar shear layer to be related to later discussions of the lobed mixer flowfield, attention in this section is also given to the initial stages of the shear-layer formation.

To ensure that the correct inlet conditions were being simulated, the predicted incoming boundary layers for both low- and high-speed streams were compared with measurements made by McCormick at 0.0254 m upstream of the plate's trailing edge. Tables 1 and 2 provide a comparison of boundary-layer parameters at this location. The tables reveal that, overall, good agreement exists between the measurements and predictions. Such good agreement

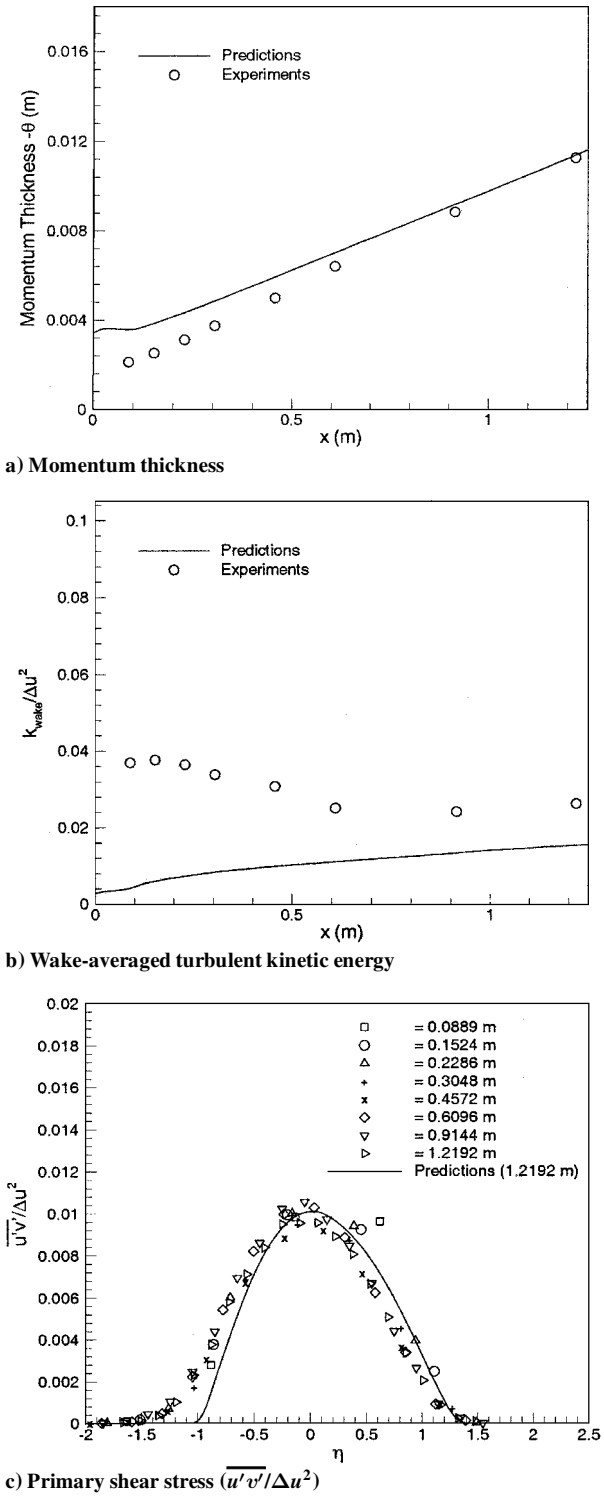

a) Momentum thickness

b) Wake-averaged turbulent kinetic energy

c) Primary shear stress ($\overline{u'v'}/\Delta u^2$)

Fig. 3 Planar shear-layer properties.

justifies comparisons to be carried out with McCormick's measurements of this particular shear layer.

Figure 3a shows the variation of the momentum thickness with downstream distance evaluated from experimental measurements and numerical predictions. The momentum thickness is defined as an integral over an area that encompasses a region with a spanwise dimension of 0.5λ (i.e., equivalent to a distance spanning a lobe trough to a lobe peak) and a height of 1λ and is given by

$$\theta = \frac{2}{\lambda}\int_0^{0.5\lambda}\int_{-5.5\lambda}^{5.5\lambda}\frac{(u-u_{\text{low}})(u_{\text{high}}-u)}{(u_{\text{high}}-u_{\text{low}})^2}\,\mathrm{d}y\,\mathrm{d}z \qquad (4)$$

The inner integral in Eq. (4) is evaluated over shear-layer regions in the interval $-5.5\lambda \le y \le 5.5\lambda$ where the streamwise component

of velocity lies within the bounds $1.01u_{\text{low}} \le u \le 0.99u_{\text{high}}$. The figure indicates that the momentum thickness is overpredicted initially. Farther downstream, the momentum thickness adopts a linear development with a spreading rate slightly lower than that given by measurements. This slight underprediction in the mixing-layer spreading rate is a well-documented feature of the k–ϵ turbulence model (e.g., Wilcox[21]). The mechanism responsible for the large discrepancies in the initial stages of the shear-layer formation also has a large effect on the wake-averaged turbulent kinetic energy. This is defined by

$$k_{\text{wake}} = \frac{2}{\lambda\delta}\int_0^{0.5\lambda}\int_{-5.5\lambda}^{5.5\lambda} k(y,z)\,dy\,dz \tag{5}$$

As with the definition of the momentum thickness, the inner integral in Eq. (5) is evaluated only where the streamwise component of velocity lies within the bounds $1.01u_{\text{low}} \le u \le 0.99u_{\text{high}}$. These bounds on the velocity are also used to define the upper (y_{upper}) and lower (y_{lower}) edges of the shear layer. The shear-layer thickness is then given by $\delta = |y_{\text{lower}} - y_{\text{upper}}|$. Results for the wake-averaged turbulent kinetic energy are shown in Fig. 3b. The turbulent kinetic energy has been nondimensionalized with respect to the square of the velocity difference between the two streams [i.e., $\Delta u = (u_{\text{high}} - u_{\text{low}})^2$]. A striking result is the very large difference in the predicted and measured turbulence levels in the formation stage of the shear layer. This is consistent with the poor comparison illustrated with the momentum thickness in the early stages. Profiles of the primary shear stress $\overline{u'v'}$ are shown in Fig. 3c. The primary shear stress is plotted against the similarity parameter η given by

$$\eta = 2(y - y_{\text{ave}})/\delta \tag{6}$$

where y_{ave} is the position of the center of the shear layer defined at the point where $u = (u_{\text{low}} + u_{\text{high}})/2$. The results reveal that, although the turbulent kinetic energy has been underpredicted by the k–ϵ model, the shear stress that controls the shear-layer spreading is well predicted in the far field.

Experimental studies by Bell and Mehta,[22] Dziomba and Fiedler,[23] and Mehta et al.[24] indicate that planar mixing layers are extremely sensitive to initial conditions in the development stages of the layer. Depending on the details of the incoming boundary layers, the measured stresses attained very different levels in the early part of the shear-layer evolution. In the study of Dziomba and Fiedler,[23] the energy spectrum was also measured for a planar shear layer with laminar boundary layers over the splitter plate. This revealed a very large and distinctive peak at a frequency corresponding to the Kelvin–Helmholtz instability. Because the Reynolds-averaged simulation does not capture this instability, it appears that the discrepancies appearing at the beginning of the shear-layer formation can be attributed to the inability to resolve this unsteady component of the flow.

To conclude this discussion, the Reynolds-averaged solution method with a k–ϵ turbulence model is well calibrated to reproduce the self-similar behavior of a planar shear layer in the far field after the Kelvin–Helmholtz instability has subsided. Inconsistencies appear between predictions and measurements, however, when comparisons are made in the initial stages of the shear-layer development particularly when the boundary layers over the splitter plate are not fully turbulent. Studies conducted on planar shear layers by other researchers have shown the shear layer to be susceptible to instabilities. Such instabilities cannot be captured with the Reynolds-averaged methodology employed in this work. In lobed mixer flows interest is usually focused on the near field because high mixing is required within the shortest duct length possible. The issues associated with the near-field modeling of the planar shear layer can therefore have important implications in simulating the lobed mixer flow.

Lobed Mixer Shear Layer

As a first step, a qualitative analysis of the numerical solution is made to ensure that the main flow features have been reproduced by the computations. Results in the form of streamlines and vortex tubes are shown in Fig. 4. The streamwise vorticity gives rise to the axially oriented vortex structure that is clearly captured in the current computations as inferred from the streamlines of Fig. 4a. The

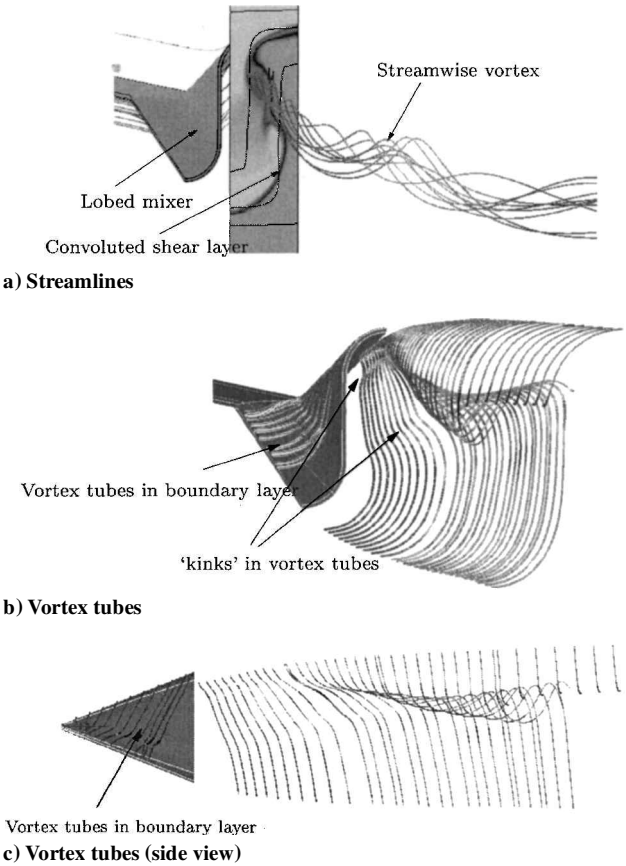

Fig. 4 Convoluted shear-layer/vortex interaction.

vorticity tubes shown in Fig. 4b clearly illustrate the convoluted nature of the shear layer. Farther downstream, the vortex tubes appear incomplete. This is a result of the propagation of the vortex tubes to the "symmetry" plane. Adjacent portions of the shear layer produced from adjacent half-lobes consequently interact at this point. This interaction of two adjacent portions of the shear layer is known as the "pinching-off" effect and was observed in McCormick's experiments. At the location where the pinching off occurs, McCormick and Bennett also observed that a sudden increase in turbulence kinetic energy arises, causing enhanced turbulent mixing downstream of this point. Figure 4c reveals that the vortex tubes are inclined at an angle perpendicular to the flow emanating from the high-speed stream. This is consistent with the flow visualizations of McCormick and Bennett and demonstrates that the mean vorticity field within the shear layer is correctly predicted.

Following the findings of the planar shear-layer results, focus in the comparisons to be presented here will be on the near-field region. Farther downstream, the shear layer is seen to reach an essentially fully mixed-out state where flow gradients are significantly reduced. It is the near-field region that determines how quickly this fully mixed-out region is reached, and consequently a clear knowledge of this part of the flow is sought. The experimental data used in the comparisons given next have been derived by averaging measurements made over the six half-lobe wavelengths covered in the measurement domain of McCormick (see Fig. 1). This provides an appropriate data set for use with the Reynolds-averaged simulations. (For easier understanding a full-lobe wavelength representation is used in the figures by reflecting the half-lobe data.)

Figure 5 presents comparisons of streamwise velocity contours between predictions and the averaged experimental data. At $x/H = 1.75$ the initial impression is a rather more diffused field in the experimental data. The rotation of the shear layer is seen to develop slower in the predictions. This is very clear from the distribution of the contours near the low-speed trough flow that are already pinching-off in the experimental data but have not quite done so at this position in the predictions. The "kinks" in the shear-layer structure created by the two streamwise vortices that form initially at the mixer's trailing edge (see the following) are also sharper in

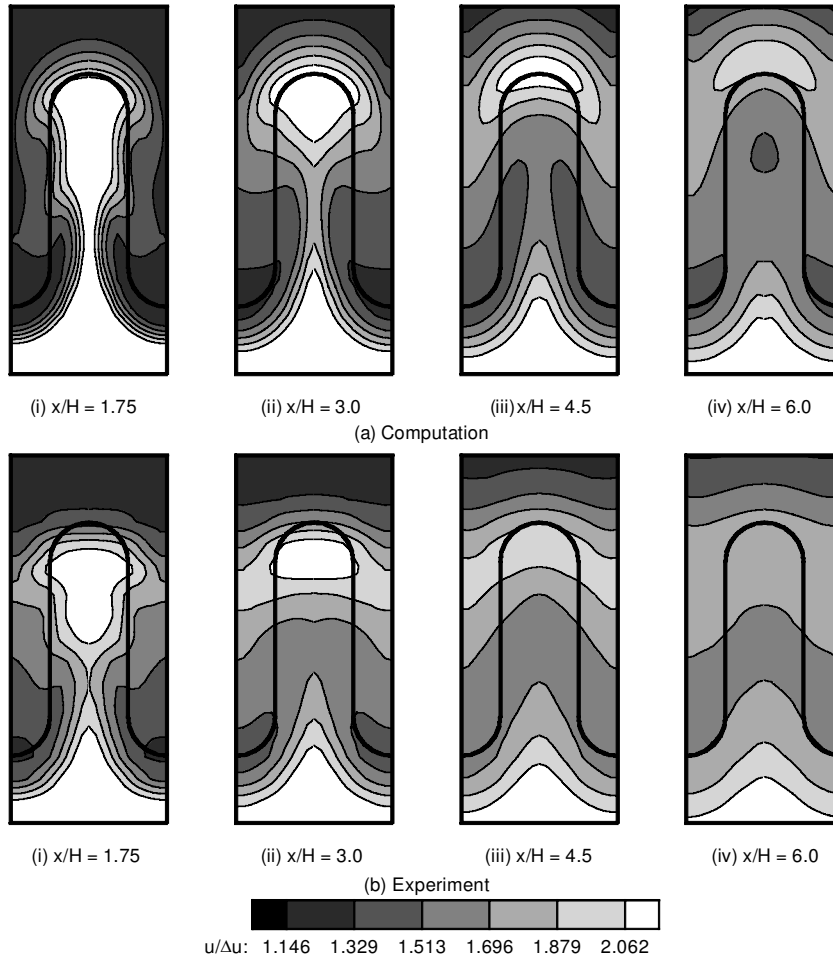

Fig. 5 Normalized streamwise velocity: a) k–ϵ model predictions and b) experimental measurements.

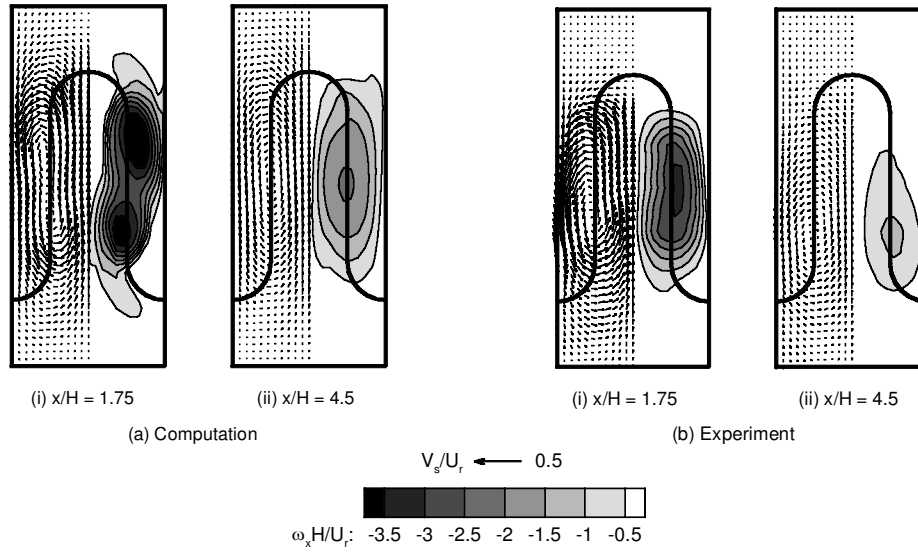

Fig. 6 Normalized streamwise vorticity contours and secondary velocity vectors: a) k–ϵ model predictions and b) experimental measurements.

the experiments than the predicted field. Another interesting feature of the predictions is the higher protrusion of the plume drawing the high-speed flow past the lobe peak. This leads to a more curved shear-layer structure near the lobe peak. Experiments show a more flattened shear-layer structure with the high-speed flow remaining well below the lobe peak. At $x/H = 3.0$ the shear-layer pinching off has occurred in the predictions. The effects seen at the preceding location are also reflected in the contour distributions here, which show a more elongated predicted shear-layer structure and a less diffused shear layer. By $x/H = 4.5$ the mixing layer in the experiments has engulfed a large portion of the flow domain. The confined high-speed flow near the lobe peak seen at the last location is no longer present, indicating a more uniformly mixed-out region. However, the effect of the pinching-off of what subsequently becomes a double-layered shear layer remains evident even at this location. This is smoothed out farther downstream at $x/H = 6.0$. Predictions at $x/H = 4.5$ still contain the region of high-speed flow near the lobe peak. Only at $x/H = 6.0$ is this seen to mix out. The results presented therefore indicate that the predicted shear-layer evolution seems to be $1.5H$ behind that seen in the experiments.

Further evidence of this behavior can be drawn from the streamwise vorticity field and secondary velocity vectors shown in Fig. 6.

At $x/H = 1.75$ clear evidence is present in the predictions of the streamwise vortices that form at the mixer's trailing edge. Bohl and Foss[25] suggested that the the creation of streamwise vorticity can be attributed to two separate mechanisms. The first mechanism is associated with the reorientation of the upstream boundary-layer vorticity. The second is caused by the spanwise pressure gradients that are established upstream of the lobed mixer penetration regions. It is believed that the streamwise vorticity observed in Fig. 6 is produced by this second mechanism. The first would produce vorticity in the opposite sense from that presented in the figure and is related to the horseshoe vortex system that is sometimes observed in lobed mixers.[4] The results presented here suggest that the contribution of the first mechanism appears to be negligible. After the boundary layers separate from the mixer surface, a vorticity field is produced that is mainly concentrated along the vertical portion of the mixer's trailing edge. The slight misalignment between the streamwise vorticity contours and the vertical mixer side wall is brought about by the rotation of the vorticity by its self-induced secondary velocity. At the same location the experimental data do not provide any indication of the two vortices seen in the predictions. Furthermore, the vorticity field seems to be weaker and more diffused. This is in line with the observation just made that experimental data indicate a faster development of the shear layer than the predictions show.

A quantitative measure of the streamwise velocity and streamwise vorticity fields is given by the axial development of momentum thickness and streamwise circulation. The momentum thickness is defined as in Eq. (4). The definition for the streamwise circulation is given by either a contour integral of the velocity component tangential to the contour line or an area integral of the streamwise component of vorticity such that

$$\Gamma_x = \oint_C \boldsymbol{v} \cdot \mathrm{d}\boldsymbol{s} = \iint_A \boldsymbol{\omega} \cdot \mathrm{d}\boldsymbol{A} \tag{7}$$

The streamwise circulation is evaluated around an integration path denoted by curve C that encompasses one half-lobe and extends from the bottom to the top wind-tunnel walls. These two quantities are shown in Figs. 7a and 7b in nondimensional form. The experimental values evaluated from the eight downstream stations used by McCormick are included.

For the momentum thickness the baseline planar mixing layer results have also been added. The variation of momentum thickness is considered first. The predicted momentum thickness captures the general trend reflected in the measured data. Initially, the momentum thickness in the lobed mixer flow shows a very rapid rise and a mixing rate higher than measured in the case of the planar shear layer. By $x/H = 6.0$ a gradual decrease follows such that by $x/H = 12.0$ the rate of mixing has dropped below the spreading rate of the baseline flat plate. The momentum thickness is underpredicted at $x/H = 1.75$ by around 20%. This is consistent with the higher level of spreading seen in the streamwise velocity contours of the measured data. In the far field the mixing rate does not fall as rapidly as the predictions imply and is consistent with the results of the planar shear layer.

The decay of the streamwise circulation is given in Fig. 7b. The streamwise circulation has been nondimensionalized using the simple inviscid theory of Skebe et al.[26] This states that at a mixer's trailing edge the streamwise circulation is given by

$$\Gamma = C_l U_r H \tan(\alpha)/2 \tag{8}$$

Using Skebe's model, McCormick[15] showed that a value of $C_l = 4$ is obtained for the mixer configuration used in this study. At the mixer trailing edge the predicted circulation agrees quite well with the inviscid theory of Skebe. The circulation then undergoes a slight increase in the predictions. Farther downstream, the measured circulation is seen to decay more rapidly than the predictions. This again proves to be consistent with results of the streamwise vorticity field presented earlier and confirms the general impression conveyed by the results so far that the predictions appear to lag the shear-layer development observed in the measurements. At $x/H = 1.75$ the calculated error is 5% increasing to 65% by $x/H = 4.5$. The delay in the decay of streamwise circulation is seen in the figure to lie in the region $0 < x/H < 1.5$, which represents a slight increase in circulation. The variation of the wake-averaged turbulent kinetic energy [as defined in Eq. (5)] is presented in Fig. 7c. As with the planar shear layer, a significant underprediction is observed. Based on the results of the planar shear layer, this underprediction is again attributed to the shear-layer instabilities that are not simulated in the computations. However, the computations correctly predict the location at which the maximum turbulence energy levels arise ($x/H = 1.75$). Farther downstream, the turbulence levels decrease as the flow mixes out.

The momentum thickness evaluated from Eq. (4) is derived from the streamwise velocity. An understanding of the processes controlling the evolution of the momentum thickness requires an

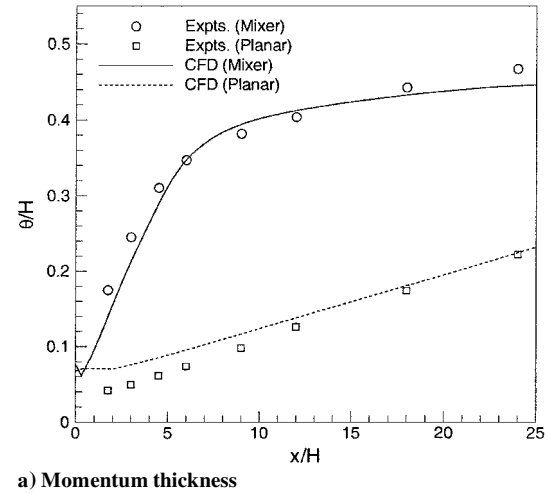

a) Momentum thickness

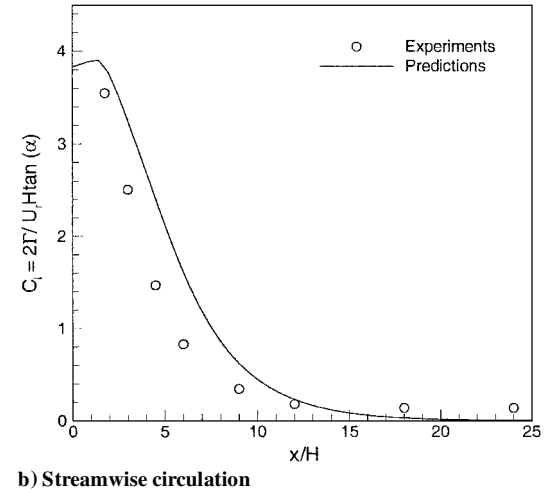

b) Streamwise circulation

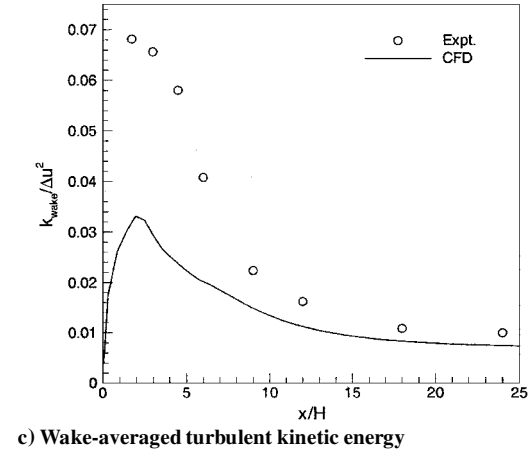

c) Wake-averaged turbulent kinetic energy

Fig. 7 Variation of global parameters with downstream distance.

understanding of the Reynolds stresses and viscous terms in the streamwise momentum equation. In this case the Reynolds stresses responsible for the diffusion of streamwise momentum are $\overline{u'v'}$ and $\overline{u'w'}$. Similarly, the streamwise circulation is evaluated from the streamwise vorticity [see Eq. (7)]. An assessment of the Reynolds stresses in the transport equation of streamwise vorticity is therefore required to understand their influence on the streamwise vorticity. To do so, the Reynolds-stress gradients [appearing in Eq. (9b)] must be evaluated. However, as remarked by Bell and Mehta,[27] computing second derivatives of the Reynolds stresses from measured data introduces very large errors. Clear evidence of this can be found in Yu and Koh.[28] Their evaluations of second derivatives of the Reynolds stresses showed results of poor quality in contrast to results of the actual Reynolds stresses. To circumvent such problems in this work, a comparison is conducted on the computed and measured Reynolds stresses rather than their gradients. Such a comparison precludes identifying the direct impact of the Reynolds stresses on the streamwise vorticity evolution. To identify which terms are most important, an understanding of the equation governing the evolution of streamwise circulation is conducted. To quantify the various turbulent stress contributions to the decay of the streamwise circulation, the following question is posed: "How does the streamwise circulation vary with the motion of the flow?" Mathematically, this translates into evaluating $\mathrm{D}\Gamma_x/\mathrm{D}t$. The variation of the streamwise circulation is then given by (cf., Batchelor[29] and Bohl and Foss[25])

$$\frac{\mathrm{D}\Gamma_x}{\mathrm{D}t} = \iint_A \left[\underbrace{\frac{\mathrm{D}\omega_x}{\mathrm{D}t} - \left(\omega_x \frac{\partial u}{\partial x} + \omega_y \frac{\partial u}{\partial y} + \omega_z \frac{\partial u}{\partial z} \right)}_{A1} \right] \mathrm{d}A_x \qquad (9a)$$

$$\frac{\mathrm{D}\Gamma_x}{\mathrm{D}t} = \iint_A \left[\underbrace{\frac{\partial}{\partial x}\left(\frac{\partial \overline{u'v'}}{\partial z} - \frac{\partial \overline{u'w'}}{\partial y} \right)}_{A2} + \underbrace{\frac{\partial^2}{\partial y \partial z}(\overline{v'^2} - \overline{w'^2})}_{A3} \right.$$

$$\left. + \underbrace{\left(\frac{\partial^2}{\partial z^2} - \frac{\partial^2}{\partial y^2} \right) \overline{v'w'}}_{A4} + \underbrace{\nu \nabla^2 \omega_x}_{A5} \right] \mathrm{d}A_x \qquad (9b)$$

For consistency, the integrals in Eq. (9b) are computed over the region enclosed by the integration path used in Eq. (7) and thus contain the vorticity fields presented in Fig. 6. The various contributions to the decay of the streamwise circulation can now be determined by evaluating the various terms on the right-hand side of Eq. (9b). In deriving Eq. (9b), the equation for streamwise vorticity has been used. This equation is derived from the analytical form of the momentum equations. To avoid the inherent numerical errors associated with the numerical computation of the second derivatives of the Reynolds stresses, the streamwise vorticity equation is derived by applying the curl operator on the discrete form of the momentum equations. Adopting this approach, and noting which terms in the momentum equations lead to the terms in the streamwise vorticity equation after the curl operator is applied, leads to an evaluation of terms A2, A3, A4, and A5 consistent with the discretization of the momentum equations. This approach has been used in deriving the results to be presented next.

Figures 8a and 8b show the contributions of the individual terms of Eqs. 9a and 9b to the variation of the nondimensional substantial derivative of the streamwise circulation. The $(\cdot)^*$ is used here to denote nondimensionalization with respect to the square of the average velocity U_r of the two streams. Figure 8a shows the variation of the substantial derivative of streamwise circulation as predicted by term A1 compared against the sum of terms A2, A3, A4, and A5. The results clearly show that term A1 and the sum of terms A2, A3, A4, and A5 are in balance. It is worth noting from this figure that near the trailing edge $(\mathrm{D}\Gamma_x/\mathrm{D}t)^*$ is slightly positive in agreement with the very slight increase in the predicted streamwise circulation seen in the results of Fig. 7b. By $x/H = 1.5$, $(\mathrm{D}\Gamma_x/\mathrm{D}t)^*$ changes sign and

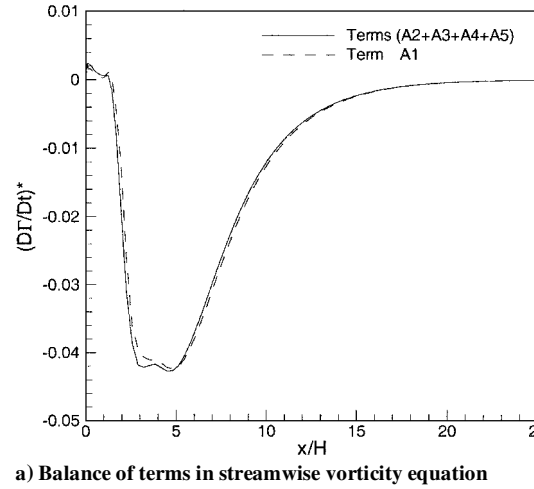

a) Balance of terms in streamwise vorticity equation

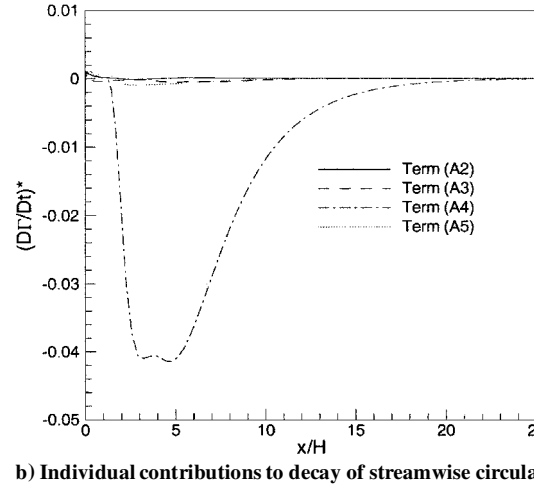

b) Individual contributions to decay of streamwise circulation

Fig. 8 Variation of $(\mathrm{D}\Gamma/\mathrm{D}t)^*$ with downstream distance for k–ϵ model.

decreases rapidly to a negative peak level by $x/H = 3.0$. This high level of decay in streamwise circulation continues up to $x/H = 5.5$, where an increase in $(\mathrm{D}\Gamma_x/\mathrm{D}t)^*$ begins, although at a rate slower than the rapid fall captured in the early stages. At $x/H = 15.0$ the variation in $(\mathrm{D}\Gamma_x/\mathrm{D}t)^*$ has more or less leveled off at a value approximately equal to zero consistent with the results presented in Fig. 7b for the nondimensional streamwise circulation.

To quantify the relative importance of the turbulent stresses to the development of the streamwise circulation, and hence vorticity field, the individual terms as classified in Eqs. (9a) and (9b) were computed and are presented in Fig. 8b. The results clearly reveal that the only significant term in this case is given by the secondary turbulent shear stress $\overline{v'w'}$. The primary shear stresses and the normal stress anisotropy have a negligible contribution to the variation of the streamwise circulation and are comparable to the contributions of the viscous stresses.

The analysis just presented yields the contributions of the different stresses to the decay of the streamwise circulation for the predicted flowfield. Such an analysis cannot be performed on the experimental data because of the large errors that would occur. A comparison of the predicted and measured Reynolds stresses is therefore conducted in order to relate the trends observed in the analysis to the experimental measurements. Initially, the primary shear stresses will be considered, and results for $-\overline{u'v'}$ and $-\overline{u'w'}$ are shown in Figs. 9 and 10, respectively, at two downstream locations within the mixing duct. At $x/H = 1.75$ the predicted $-\overline{u'v'}$ shear-stress contours exhibit peak negative values near the lobe peaks and troughs where velocity gradients are predominantly aligned along the y axis. Two regions of positive extrema exist along the vertical side walls, and these coincide with the two "kinks" of the shear-layer structure seen in the streamwise velocity contours. Similar features exist in the experimental data, although extrema near the lobe peak are

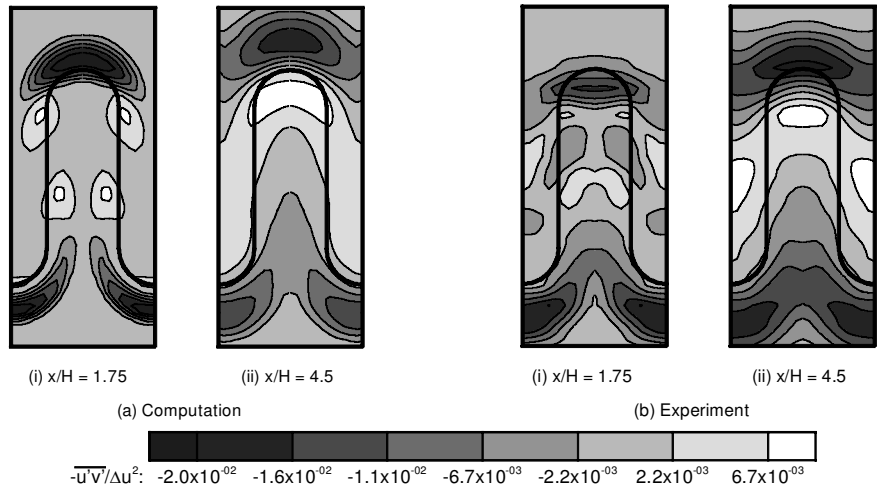

Fig. 9 Normalized primary shear stress ($-\overline{u'v'}/\Delta u^2$): a) k–ϵ model predictions and b) experimental measurements.

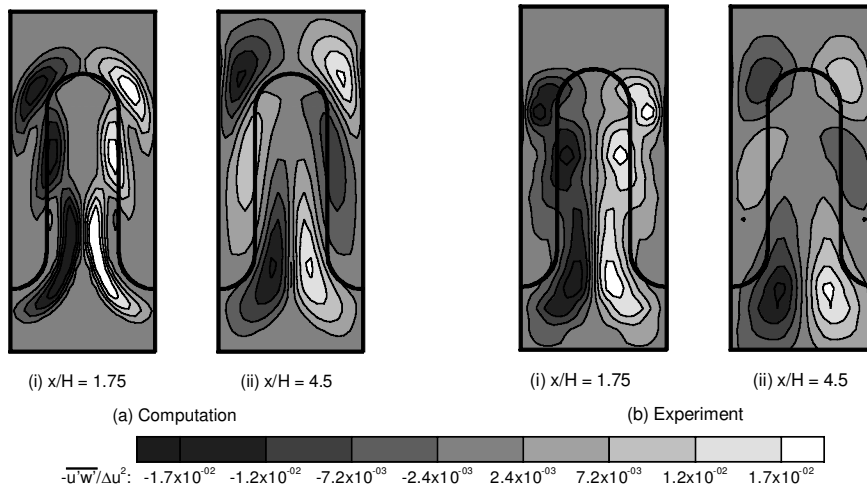

Fig. 10 Normalized primary shear stress ($-\overline{u'w'}/\Delta u^2$): a) k–ϵ model predictions and b) experimental measurements.

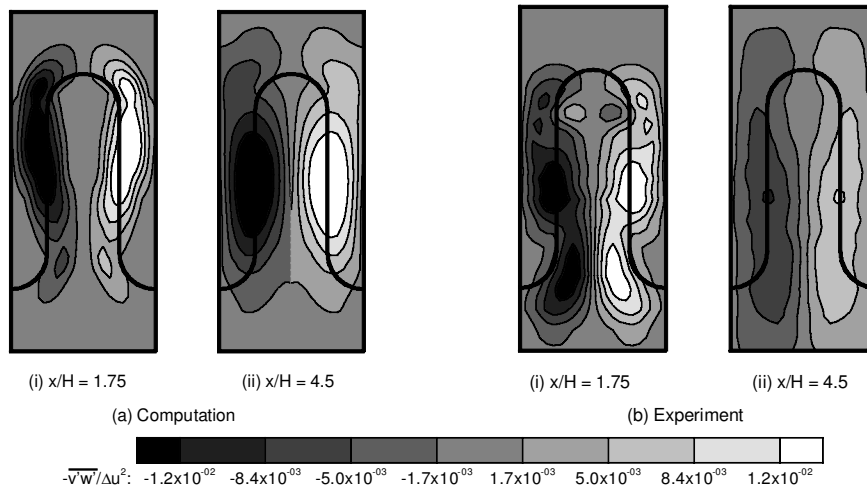

Fig. 11 Normalized secondary shear stress ($-\overline{v'w'}/\Delta u^2$): a) k–ϵ model predictions and b) experimental measurements.

substantially less widespread and are lower in relation to the predictions. In the vicinity of the lobe troughs, the experimental data show a more diffused distribution of shear stresses. These results are consistent with the discussion of the streamwise velocity contours just presented, and the distinctly different distribution in comparison with the predictions confirms this point. At $x/H = 4.5$ the more highly stretched shear layer of the predictions is reflected in the positive shear-stress contours lying between the two-layered shear layer. Comparisons of the second primary shear stress shown in Fig. 10 illustrate essentially the same level of agreement discussed for the $-\overline{u'v'}$ shear stress. Accordingly, it can be concluded that the primary shear stresses are well predicted but are generally less spread out than the experimental data.

Plots of the secondary shear stress $-\overline{v'w'}$ presented in Fig. 11 reveal relatively poorer agreement between predictions and experiments in comparison to the primary shear stresses, particularly in the farther downstream region. At $x/H = 1.75$ the secondary shear stress is seen to be concentrated along the vertical mixer walls. The experimental data reveal the contours are in a relatively lower position, and this is indicative of the lower vortex position as depicted by

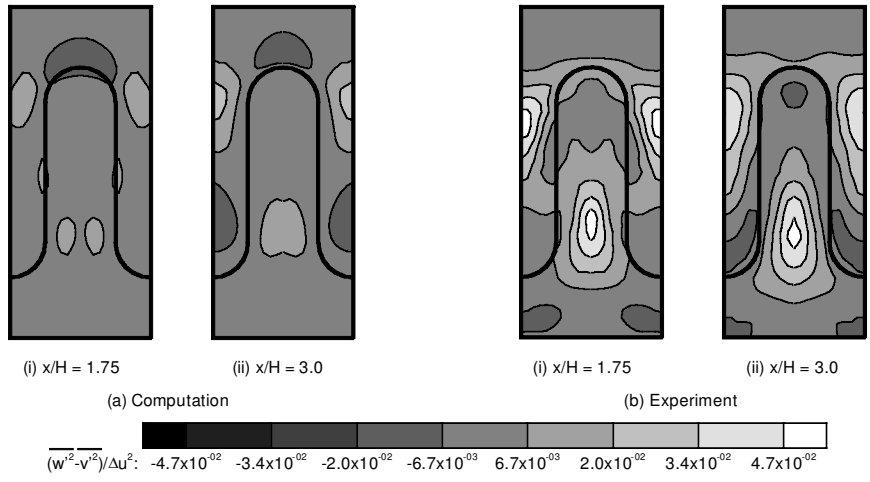

Fig. 12 Nondimensionalized normal stress anisotropy ($\overline{w'^2} - \overline{v'^2}/\Delta u^2$): a) k–ϵ model predictions and b) experimental measurements.

the velocity contours discussed earlier. The double-peaked distribution seen in the experiments is also a distinct feature not present in the simulations in which a plateau of peak shear-stress levels is predicted. Considering the faster development of the shear layer in the experiments and the highly distorted shear-layer structure seen in the streamwise velocity contours, it appears that these double-peaked regions arise following the pinching-off mechanism that split the high stress levels into two separate regions. This pinching-off mechanism is much weaker in the simulations, a fact supported by the weaker kinks in the shear layer, causing a modified shear-stress distribution. At $x/H = 3.0$ the processes taking place upstream lead to more vertically elongated shear-stress contours in the experiments. Peak shear-stress levels are additionally lower than in the predictions and continue to decay at a more rapid rate than the simulations predict.

It is now possible to explain why the momentum thickness can be predicted more accurately than the streamwise circulation with the k–ϵ turbulence model. Although the momentum thickness is a function of the streamwise velocity and thus depends on the primary shear stresses $\overline{u'v'}$ and $\overline{u'w'}$, the streamwise circulation development is strongly dependent on the secondary shear stress $\overline{v'w'}$ as has been indicated by the preceding analysis. A standard linear k–ϵ model is calibrated to provide good predictions of the primary shear stress $\overline{u'v'}$ of a planar shear layer. For a convoluted shear layer $\overline{u'w'}$ would be expected to play a similar role to $\overline{u'v'}$ in the mixing of the shear layer, and consequently a good prediction of the momentum thickness is expected. The secondary shear stress $\overline{v'w'}$ has no direct analog in a planar shear layer, and thus predicting the decay of streamwise circulation proves to be more difficult than the momentum thickness. The negligible contribution arising from the primary shear stresses (term A2) to the streamwise circulation can be attributed to the streamwise derivative appearing in this term. In general, the convoluted shear layers of lobed mixers will exhibit much larger gradients in the plane perpendicular to the streamwise direction. Therefore, terms A3 and A4 can be expected to dominate term A2. However, from the analysis just conducted the normal stress anisotropy also has a negligible contribution. To evaluate whether this is a feature of the flow or an artifact of the k–ϵ turbulence model, a comparison of the normal stress anisotropy is presented in Fig. 12. The turbulence model predictions reveal that a very small degree of anisotropy is predicted by the k–ϵ model throughout the flowfield. Highest values appear to occur near the regions where the pinched-off behavior takes place. Comparisons with measurements nevertheless show that anisotropies in the pinched-off regions are significantly underpredicted by the k–ϵ turbulence model. The experiments show a very rapid fall in the levels of anisotropy between $x/H = 1.75$ and 4.5. It is therefore expected that the effects of anisotropy are predominant in the early stages of the shear-layer development. These results illustrate the poor prediction of term A3 of Eq. (9b) by this turbulence model for this flow. This demonstrates that the circulation decay rate is incorrectly predicted as a result of the inability to correctly resolve the secondary shear stress and the normal-stress anisotropy.

Conclusions

A detailed validation study of a k–ϵ turbulence model prediction for an incompressible lobed mixer flowfield has been presented. The development of the predicted mean streamwise velocity and mean streamwise vorticity with distance downstream from the mixer showed a lag of $x/H = 1.75$ with respect to measured data. The accuracy of the predicted streamwise velocity and streamwise vorticity fields were quantified by evaluating the momentum thickness and streamwise circulation respectively. The momentum thickness was predicted with an accuracy of 20%. The streamwise circulation was computed with a substantially larger error of 65%.

An analysis of the governing flow equations revealed that the momentum thickness is controlled by the primary shear stresses $\overline{u'v'}$ and $\overline{u'w'}$. As illustrated in this study, the k–ϵ turbulence model is calibrated to provide good predictions of the primary shear stress in a planar shear layer. Both the $\overline{u'v'}$ and $\overline{u'w'}$ stresses play a similar role in a convoluted shear layer. These stresses are therefore well predicted by the k–ϵ turbulence model. In contrast, the streamwise circulation is strongly dependent on the secondary shear stress $\overline{v'w'}$ and the normal stress anisotropy ($w'^2 - v'^2$), both of which are not well predicted by the model. Consequently, the computed momentum thickness is predicted more accurately in comparison to the streamwise circulation.

The analysis conducted in this study has shown that, despite the difficulties in correctly predicting the turbulence field, mean quantities and trends of global parameters are generally in good agreement with measured data. The study suggests that a turbulence model based on a higher level of Reynolds-stress closure can lead to improved predictions for the decay rate of the streamwise circulation. Preliminary exploration using a quadratic nonlinear form of the k–ϵ turbulence model for another lobed mixer configuration has already been conducted. A more thorough validation study of the quadratic nonlinear model for the mixer configuration used in this study will appear in a later publication.

Acknowledgments

The authors acknowledge funding support for the research work reported here from the Engineering and Physical Sciences Research Council (UK), Grant GR/L17863. Financial assistance and technical review monitoring was also provided by Rolls–Royce and DERA; the authors thank in particular Paul Strange, Rolls–Royce, and Craig Mead, DERA. The first author thanks Duane McCormick for providing the experimental data used in this study.

References

[1] Ho, C.-M., and Huerre, P., "Perturbed Free Shear Layers," *Annual Review of Fluid Mechanics*, Vol. 16, 1984, pp. 365–424.

[2] Shumpert, P. K., "An Experimental Model Investigation of Turbofan Engine Internal Exhaust Gas Mixer Configurations," AIAA Paper 80-0228, 1980.

[3] Bevilaqua, P. M., "Evaluation of Hypermixing for Thrust Augmenting Ejectors," *Journal of Aircraft*, Vol. 11, No. 6, 1978, pp. 348–354.

[4]Paterson, R. W., "Turbofan Forced Mixer-Nozzle Internal Flow Field, Part 1—A Benchmark Experimental Study," NASA CR 3492, 1982.

[5]Strickland, J. H., Selerland, T., and Karagozian, A. R., "Numerical Simulations of a Lobed Fuel Injector," *Physics of Fluids*, Vol. 10, No. 11, 1998, pp. 2950–2964.

[6]Koutmos, P., and McGuirk, J. J., "Turbofan Forced Mixer/Nozzle Temperature and Flow Field Modelling," *International Journal of Heat and Mass Transfer*, Vol. 32, No. 6, 1989, pp. 1141–1153.

[7]Launder, B. E., and Spalding, D. B., "The Numerical Computation of Turbulent Flows," *Computer Methods in Applied Mechanics and Engineering*, Vol. 3, 1974, pp. 269–289.

[8]Malecki, R. E., and Lord, W. K., "Navier–Stokes Analysis of a Lobed Mixer and Nozzle," AIAA Paper 90-0453, 1990.

[9]Abolfadl, M. A., and Sehra, A. K., "Application of Three-Dimensional Viscous Analysis to Turbofan Forced Mixers," AIAA Paper 91-0131, 1991.

[10]Tsui, Y.-Y., and Wu, P.-W., "Investigation of the Mixing Flow Structure in Multilobe Mixers," *AIAA Journal*, Vol. 34, No. 7, 1996, pp. 1386–1391.

[11]O'Sullivan, M. N., Krasnodebski, J. K., Waitz, I. A., Greitzer, E. M., Tan, C. S., and Dawes, W. N., "Computational Study of Viscous Effects on Lobed Mixer Flow Features and Performance," *Journal of Propulsion and Power*, Vol. 12, No. 3, 1996, pp. 449–456.

[12]Salman, H., McGuirk, J. J., and Page, G. J., "A Numerical Study of Vortex Interactions in Lobed Mixer Flow Fields," AIAA Paper 99-3409, June 1999.

[13]Yu, S. C. M., and Yip, T. H., "Measurements of Velocities in the near Field of a Lobed Forced Mixer Trailing Edge," *Aeronautical Journal*, Vol. 101, No. 1003, 1997, pp. 121–129.

[14]McCormick, D. C., and Bennett, J. C., Jr., "Vortical and Turbulent Structure of a Lobed Mixer Free Shear Layer," *AIAA Journal*, Vol. 32, No. 9, 1994, pp. 1852–1859.

[15]McCormick, D. C., "Vortical and Turbulent Structure of Planar and Lobed Mixer Free-Shear Layers," Ph.D. Dissertation, Dept. of Mechanical Engineering, Univ. of Connecticut, Storrs, CT, May 1992.

[16]Eckerle, W. A., Sheibani, H., and Awad, J., "Experimental Measurement of the Vortex Development of a Lobed Forced Mixer," *Journal of Engineering for Gas Turbines and Power*, Vol. 114, Jan. 1992, pp. 63–71.

[17]Yu, S. C. M., Yeo, J. H., and Teh, J. K. L., "Velocity Measurements Downstream of a Lobed-Forced Mixer with Different Trailing-Edge Configurations," *Journal of Propulsion and Power*, Vol. 11, No. 1, 1995, pp. 87–97.

[18]Page, G. J., Zhao, H., and McGuirk, J. J., "A Parallel Multiblock Reynolds Averaged Navier–Stokes Method for Propulsion Installation Applications," *12th International Symposium on Air Breathing Engines*, Vol. 1, 1995, pp. 864–874.

[19]Salman, H., "Numerical Simulation of Streamwise Vorticity Enhanced Mixing," Ph.D. Dissertation, Dept. of Aeronautical and Automotive Engineering, Loughborough Univ., Loughborough, England, U.K., Jan. 2001.

[20]Rollin, G., Duparcq, J. L., and Joubert, H., "Application of a 3D Navier–Stokes Solver to Analyse the Performance of a Lobed Mixer," *ICAS Proceedings*, Vol. 3, 1994, pp. 2128–2135.

[21]Wilcox, D. C., *Turbulence Modeling for CFD*, DCW Industries, Inc., 1994, pp. 137–147.

[22]Bell, J. H., and Mehta, R. D., "Development of a Two-Stream Mixing Layer from Tripped and Untripped Boundary Layers," *AIAA Journal*, Vol. 28, No. 12, 1990, pp. 2034–2042.

[23]Dziomba, B., and Fiedler, H. E., "Effect of Initial Conditions on Two-Dimensional Free Shear Layers," *Journal of Fluid Mechanics*, Vol. 152, March 1985, pp. 419–442.

[24]Mehta, R. D., Inoue, O., King, L. S., and Bell, J. H., "Comparison of Experimental and Computational Techniques for Plane Mixing Layers," *Physics of Fluids*, Vol. 30, No. 7, 1987, pp. 2054–2062.

[25]Bohl, D. G., and Foss, J. F., "Near Exit Plane Effects Caused by Primary and Primary-Plus-Secondary Tabs," *AIAA Journal*, Vol. 37, No. 2, 1999, pp. 192–201.

[26]Skebe, S. A., Paterson, R. W., and Barber, T. J., "Experimental Investigation of Three-Dimensional Forced Mixer Lobe Flow Fields," AIAA Paper 88-3785-CP, 1988.

[27]Bell, J. H., and Mehta, R. D., "Measurements of the Streamwise Vortical Structures in a Plane Mixing Layer," *Journal of Fluid Mechanics*, Vol. 239, June 1992, pp. 213–248.

[28]Yu, S. C. M., and Koh, P. K., "An Experimental Investigation of Two-Stream Mixing Flow with a Single Delta Tab," *International Journal of Heat and Fluid Flow*, Vol. 22, 2001, pp. 62–71.

[29]Batchelor, G. K., *An Introduction to Fluid Dynamics*, Cambridge Univ. Press, Cambridge, England, U.K., 1994, pp. 266, 267.

R. M. C. So
Associate Editor